Electronic structure, chemical bonding, and optical properties of paraelectric $BaTiO_3$

Sonali Saha and T. P. Sinha
Department of Physics, Bose Institute, 93/1, Acharya Prafulla Chandra Road, Calcutta 700009, India

Abhijit Mookerjee
S. N. Bose National Centre for Basic Sciences, JD Block, Sector 3, Salt Lake City, Calcutta 700091, India
(Received 22 November 1999; revised manuscript received 23 May 2000)

The electronic-energy band structure, site, and angular-momentum decomposed density of states (DOS) and charge-density contours of perovskite $BaTiO_3$ in the paraelectric phase are calculated by the first-principles tight-binding linear muffin-tin orbitals method with the atomic-sphere approximation using density-functional theory in its local-density approximation. The calculated band structure shows a direct band gap of 1.2 eV at the Γ point in the Brillouin zone. The total DOS is compared to the experimental x-ray photoemission spectrum. From the DOS analysis, as well as charge-density studies, we conclude that the bonding between Ba and TiO_3 is mainly ionic and that the TiO_3 entities bond covalently. Using the projected DOS and band structure we have analyzed the interband contribution to the optical properties of $BaTiO_3$. The real and imaginary parts of the dielectric function and hence the optical constants (such as the reflectivity, refractive index, extinction coefficient, absorption coefficient, and the electron energy-loss spectrum) are calculated. The calculated spectra are compared with the experimental results for $BaTiO_3$ at room temperature in the ferroelectric phase and are found to be in good agreement with the experimental data in the low-energy regions. The role of band-structure calculation as regards the optical properties of $BaTiO_3$ is discussed.

I. INTRODUCTION

Ferroelectric and related materials having the chemical formula ABO_3 have been the subjects of extensive investigation, both because of their technical importance and because of the fundamental interest in the physics of their phase transitions.[1] Within this family of materials, one finds transitions to a wide variety of low-symmetry phases, including ferroelectric and antiferroelectric transitions. The ideal structure is cubic perovskite, where the *A* and *B* cations are arranged on a simple cubic lattice and the O ions lie on the face centers nearest the (typically transition metal) *B* cations. Thus the *B* cations are at the centers of O octahedra, while the *A* cations lie in a larger 12-fold-coordinated sites. This ideal structure displays a wide variety of structural instabilities in the various materials. These may involve rotations and distortions of the O octahedra as well as displacements of the cations from their ideal sites. The interplay of these instabilities accounts for the rich variety of ferroelectric and antiferroelectric behaviors.

$BaTiO_3$ is among the most extensively studied systems in this class. It transforms from the high-temperature high-symmetry paraelectric cubic perovskite phase to slightly distorted ferroelectric structures with tetragonal, orthorhombic and rhombohedral symmetries.[1] The cubic perovskite structure exists above 120 °C. Below 120 °C it transforms to the tetragonal phase which exists down to 5 °C. Since the discovery of ferroelectricity in $BaTiO_3$, a large number of investigations have been carried out to study its various properties,[2–9] no theoretical investigations of optical properties based upon the first-principles band-structure calculations have been reported to our knowledge.

Spitzer *et al.*[3] have measured the infrared reflectivity spectra of $BaTiO_3$ at room temperature and from these data they have calculated the principal dielectric-response functions using Kramers-Kronig relations. Investigations have been carried out to study the structural,[10] dielectric,[10] elastic, and thermal properties,[10] the infrared,[2] and the Raman[4,6] as well as electron-spin resonance[11] spectra of $BaTiO_3$. Recent studies[12–14] on nanocrystalline powders of $BaTiO_3$ have shown that the tetragonal ferroelectric structure disappears below a critical size of the particle, leading to the cubic phase.

In the present study, the electronic structure and optical properties of cubic perovskite $BaTiO_3$ in the paraelectric phase are calculated by the first-principles tight-binding linearized muffin-tin orbital (TB-LMTO) method with the atomic-sphere approximation (ASA) using density-functional theory in its local-density approximation (LDA).[15] The first-principles density-functional calculations offer an attractive approach for enhancing our microscopic understanding of perovskites. The all-electron full-potential linearized augmented plane-wave method has been used by several groups to study ferroelectricity in perovskites within the LDA.[16–19] Recently, King-Smith and Vanderbilt performed a systematic study of structural and dynamical properties and energy surfaces for eight common perovskites using the first principles ultrasoft pseudopotential method and the LDA.[20,21] These calculations demonstrate that ferroelectricity in the perovskites reflects a delicate balance between long-range electrostatic forces which favor the ferroelectric state and short-range repulsions which favor the cubic phase. In the next sections, the computational details regarding the methods used in our calculations of the electronic structure and optical properties are described. Finally, the calculated results are compared with available experimental data.[8,9]

II. COMPUTATIONAL DETAILS

The crystal structure of $BaTiO_3$ in the para- and ferroelectric phases has been studied experimentally using various

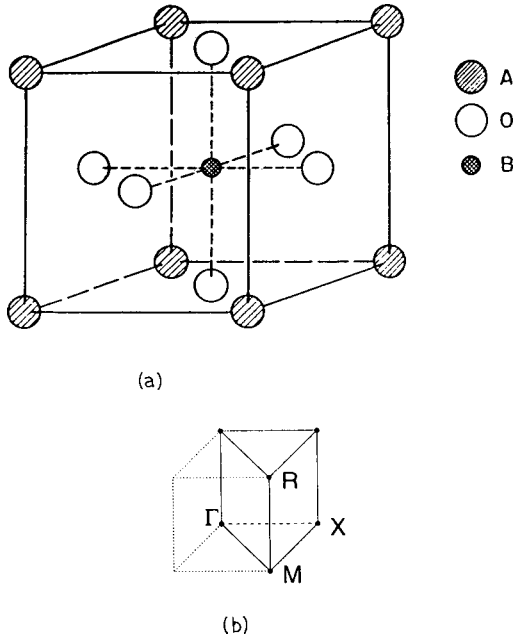

FIG. 1. (a) The cubic unit cell of $BaTiO_3$. (b) The Brillouin zone for the cubic $BaTiO_3$.

techniques.[10] The paraelectric phase is cubic and belongs to the space group $Pm(3)m$. The ferroelectric phase has the tetragonal structure with a small tetragonal distortion ($c/a = 1.01$).[10] The cubic unit cell contains one molecule with the Ba sitting at the origin $(0.0,0.0,0.0)a$, the Ti at the body center $(0.5,0.5,0.5)a$ and the three oxygen atoms at the three face centers $(0.5,0.5,0.0)a$, $(0.0,0.5,0.5)a$, and $(0.5,0.0,0.5)a$. The lattice constant is 7.57 a.u., taken from the experimental results of Jona and Shirane.[10] Figure 1(a) shows the unit cell and Fig. 1(b) the Brilluoin zone of $BaTiO_3$ for this structure.

We present here electronic structure calculations made using the TB-LMTO. The calculations were done within the ASA. The basis sets used here comprised of augmented linear muffin-tin orbitals. Within the atomic spheres, the basis functions, the charge density and the potential are expanded in symmetry-adapted, spherical harmonics together with a radial function. Basis functions up to $l_{\max}=3$ for Ba and $l_{\max}=2$ for Ti and O were used. The calculations were carried out within the LDA and the radial part of the basis was obtained by solving a Schrödinger-like Kohn-Sham equation[22] in which the scalar relativistic corrections were incorporated. The von Barth-Hedin exchange potential[23] was used. The atomic-sphere overlap was $<12\%$. Brillouin-zone integration was carried out using the tetrahedron method[24] using a mesh of about 500 symmetry-reduced points. The Ba $6p$, the O $3s$ and $3d$ orbitals were downfolded and do not contribute to the dimension of the Hamiltonian (H) and the overlap (O) matrices, but carry charge. This downfolding avoided the appearance of ghost bands.

The linear response of the system to an external electromagnetic field with a small wave vector is measured through the complex dielectric function $\epsilon(\omega)$. The frequencies of interest to us will be well above those of phonons, so we consider the electronic excitations alone. This we do within the random-phase approximation. Local-field and lifetime effects will be neglected. Lifetime broadening will be reintroduced subsequently phenomenologically by convoluting the absorptive part of $\epsilon(\omega)$ with a Lorentzian with a full width at half maximum (FWHM) of 8×10^{-4} Ryd at the photon energy of 0.073 Ryd increasing quadratically with photon energy, as suggested by Ravindran *et al.*[25] The cubic nature of $BaTiO_3$ leads to a diagonal and isotropic dielectric tensor. The imaginary part $\epsilon''(\omega)$ of the dielectric function $\epsilon(\omega)$ is then given by

$$\epsilon''(\omega)=\left(\frac{Ve^2}{2\pi\hbar m^2\omega^2}\right)\int d^3\mathbf{k}\sum_{nn'}|\langle\mathbf{k}n|\mathbf{p}|\mathbf{k}n'\rangle|^2 \times f(\mathbf{k}n)(1-f(\mathbf{k}n'))\delta(E_{\mathbf{k}n}-E_{\mathbf{k}n'}-\hbar\omega). \quad (1)$$

Here $\hbar\omega$ is the energy of the incident photon, $\mathbf{p}$ is the momentum operator $(\hbar/i)\partial/\partial x$, $|\mathbf{k}n\rangle$ is a crystal wave function and $f(\mathbf{k}n)$ is the Fermi function. The other symbols have their usual meanings. It is often easier to convert from the reciprocal-space $\mathbf{k}$ as the variable of integration to the energy E and from the band index n to the LMTO indices L,α, where $L=(l,m)$ are angular momenta and α labels the particular atom in the unit cell. The expression (1) then becomes

$$\epsilon''(\omega)=\frac{A}{\omega^2}\int dE\sum_{LL',\alpha\alpha'}T_{LL'}^{\alpha\alpha'}(E,\omega)n_L^{\alpha}(E) \times n_{L'}^{\alpha'}(E+\hbar\omega)f(E)(1-f(E')), \quad (2)$$

where A is a constant, $n_L(E)$ is the angular-momentum projected density of states, $f(E)$ is the Fermi function, and the transition matrix $T_{LL'}(E,\omega)$ is given by

$$T_{LL'}(E,\omega)=\left|\int d^3r\,\phi_L^*(E,\mathbf{r})\frac{\partial}{\partial x}\phi_{L'}(E+\hbar\omega,\mathbf{r})\right|^2.$$

The matrix element is evaluated over the atomic spheres. In addition to the lifetime broadening which is introduced at this stage, an additional Gaussian broadening due to instrumental resolution of FWHM of 4×10^{-4} Ryd was also incorporated.

The real part $\epsilon'(\omega)$ of the dielectric function $\epsilon(\omega)$ follows from the Kramers-Kronig relationship. All optical constants may now be derived from this. If we assume orientation of the crystal surface parallel to the optical axis, the reflectivity $R(\omega)$ follows directly from Fresnel's formula:

$$R(\omega)=\left|\frac{\sqrt{\epsilon(\omega)}-1}{\sqrt{\epsilon(\omega)}+1}\right|^2.$$

Expressions for the absorption coefficient $I(\omega)$, extinction coefficient $k(\omega)$, energy-loss spectrum $L(\omega)$, and the refractive index $n(\omega)$, now follow immediately:

$$I(\omega)=\sqrt{2}\omega[\sqrt{\epsilon'(\omega)^2+\epsilon''(\omega)^2}-\epsilon'(\omega)]^{1/2},$$

$$k(\omega)=I(\omega)/2\omega,$$

$$L(\omega)=\epsilon''(\omega)/[\epsilon'(\omega)^2+\epsilon''(\omega)^2],$$

$$n(\omega)=(1/\sqrt{2})[\sqrt{\epsilon'(\omega)^2+\epsilon''(\omega)^2}+\epsilon'(\omega)]^{1/2}. \quad (3)$$

It is to be noted that for the interpretation of the optical spectra of systems, it does not seem realistic to give a single

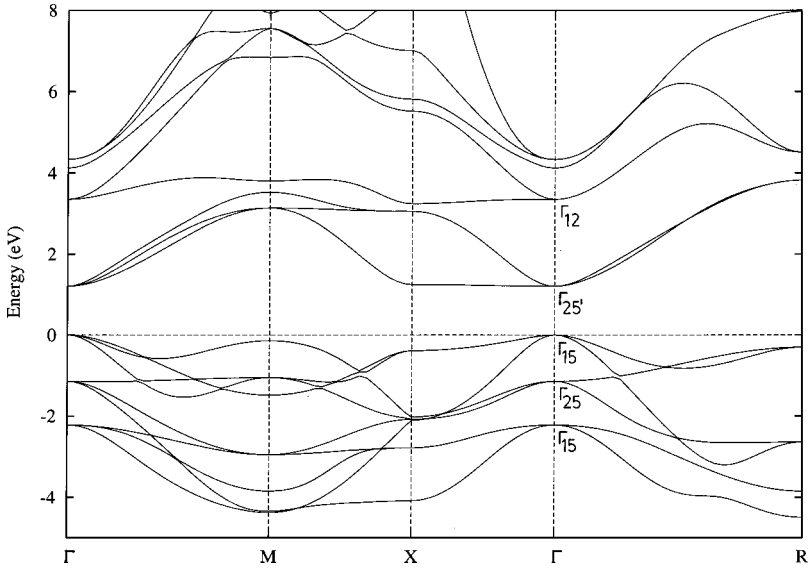

FIG. 2. The calculated energy-band structure for $BaTiO_3$. The zero of the energy was set at the top of the valence band.

transition assignment to the peaks present in a crystal reflection spectrum since many transitions (direct to indirect) may be found in the band structure with an energy corresponding to the peak, and since states away from the lines and point of symmetry could contribute to the reflectivity. Therefore, the symmetry-allowed transition energies lead to an incomplete description of the optical spectrum. We have generated theoretical curves using the customary approximation made to interpret the optical spectra from band-structure calculations, namely by considering the imaginary part $\epsilon''(\omega)$ of the optical dielectric constant $\epsilon(\omega)$ as proportional to the joint density of states weighted by ω^{-2}. Although the room-temperature phase of $BaTiO_3$ has the tetragonal structure with a small tetragonal distortion, we consider its optical spectra to be not much different from the cubic phase and will compare the calculated results with the room-temperature experimental data of Bauerle *et al.*[8]

III. RESULTS AND DISCUSSION

A. Band structure and density of states

Since the optical spectra are calculated from interband transitions, we first describe our calculated electronic structure. The calculated band structure for paraelectric $BaTiO_3$ in the high-symmetry directions in the Brillouin zone is shown in Fig. 2. The energy scale is in eV, and the origin of energy was arbitrarily set to be at the valence band maximum. In the figure we find a large dispersion of the bands. Nine valence bands are derived from O $2p$ orbitals. These are separated by a direct gap of 1.2 eV (at the Γ point) from the transition-metal d-derived conduction band. This gap is somewhat lower than the experimental band gap 3.2 eV for $BaTiO_3$.[6] The origin of this discrepancy may be the local-density approximation which underestimates the band gaps even for insulators. The nine valence bands at the Γ point are the three triply degenerate levels (Γ_{15}, Γ_{25}, and Γ_{15}) separated by energies of 1.14 ($\Gamma_{15}-\Gamma_{25}$) and 1.09 eV ($\Gamma_{25}-\Gamma_{15}$). These splittings are produced by the crystal field and the electrostatic interaction between O $2p$ orbitals. In the conduction band the triply ($\Gamma_{25'}$) and doubly (Γ_{12}) degenerate levels represent t_{2g} and e_g states of Ti $3d$ orbitals separated by energy of 2.15 eV. A visual comparison of our band-

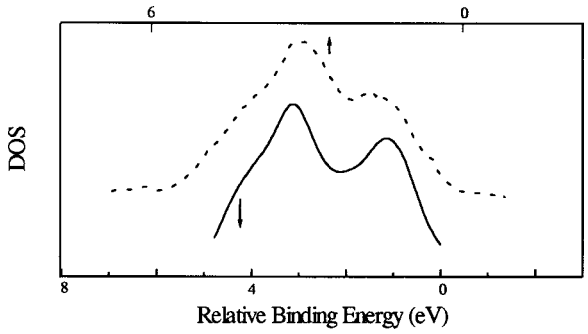

FIG. 3. The calculated total density of states (DOS) in the valence region and the XPS spectrum (Ref. 9) for $BaTiO_3$: continuous line indicates theoretical, dotted line indicates experimental.

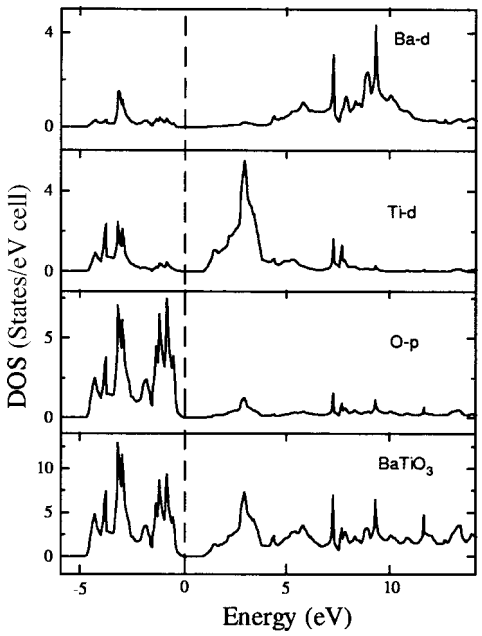

FIG. 4. The angular-momentum and site-projected density of states for $BaTiO_3$. The zero of the energy scale shows the position of the Fermi level.

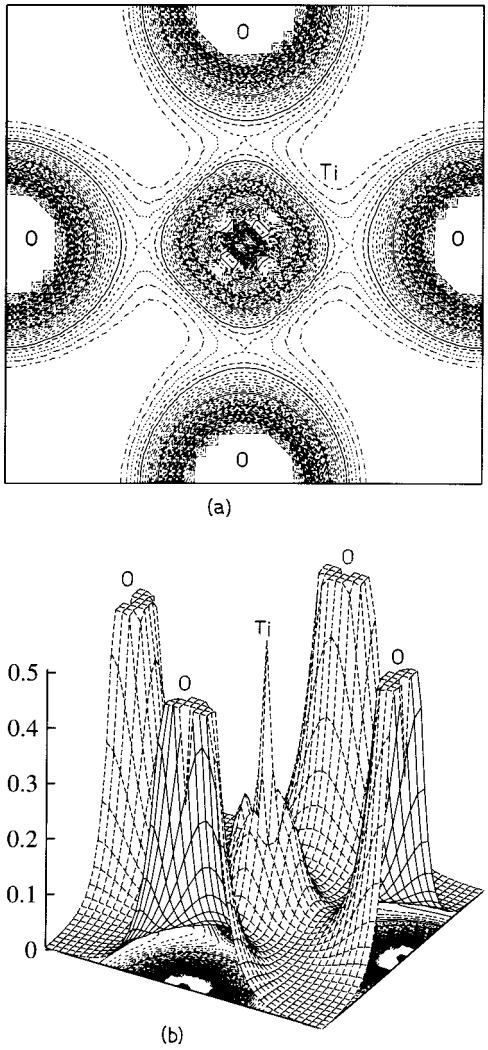

FIG. 5. The valence charge density contour for cubic $BaTiO_3$ in the (200) plane (a) in two dimensions (b) in three dimensions.

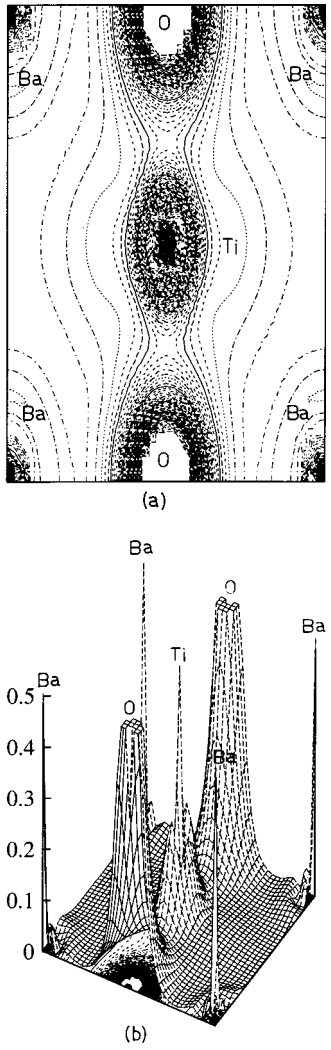

FIG. 6. The valence charge density contour for cubic $BaTiO_3$ in the (110) plane (a) in two dimensions (b) in three dimensions.

structure results against those of King-Smith and Vanderbilt on $BaTiO_3$ shows almost no discernible difference except that they have obtained a direct band gap of 1.8 eV at the Γ point using the pseudopotential method.[20] We have also performed the calculations with the theoretical lattice constant ($a = 7.43$ a.u.) but the band gap and the nature of the band structure remained the same with a slight shifting in the positions of Ti Γ_{12} and O Γ_{25} states.

The calculated total DOS for $BaTiO_3$ in the valence-band region along with experimental results [the x-ray photoemission spectroscopy (XPS) spectrum] (Ref. 9) are shown in Fig. 3. The calculated DOS was convoluted with a Lorentzian of 0.94 eV full width at half maximum. The valence-band maximum is set to zero on the energy scale. Our DOS exhibits sharper peaks than the experimental spectrum (Fig. 3), since we have not included the lifetime broadening in our DOS curve. The experimental band width is 6 eV whereas our calculated result gives a band of width 4.8 eV. This reduction of band width is due to muffin-tin approximation.[26] To get more insight into the valence-band spectra near the Fermi level, we have shown the angular-momentum and site-decomposed DOS in Fig. 4. There exists a strong *p-d* hybridization as is evident from this figure. The Ti $3d$ contribution

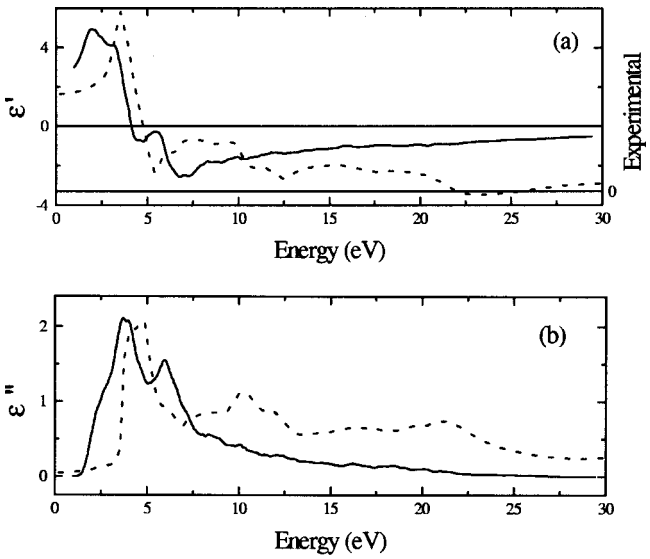

FIG. 7. The optical spectrum of the dielectric constant as a function of the photon energy for paraelectric $BaTiO_3$, (a) the real part $\epsilon'(\omega)$ and and (b) the imaginary part $\epsilon''(\omega)$ of the dielectric function $\epsilon(\omega)$: dotted line is experimental (Ref. 8), continuous line is theoretical.

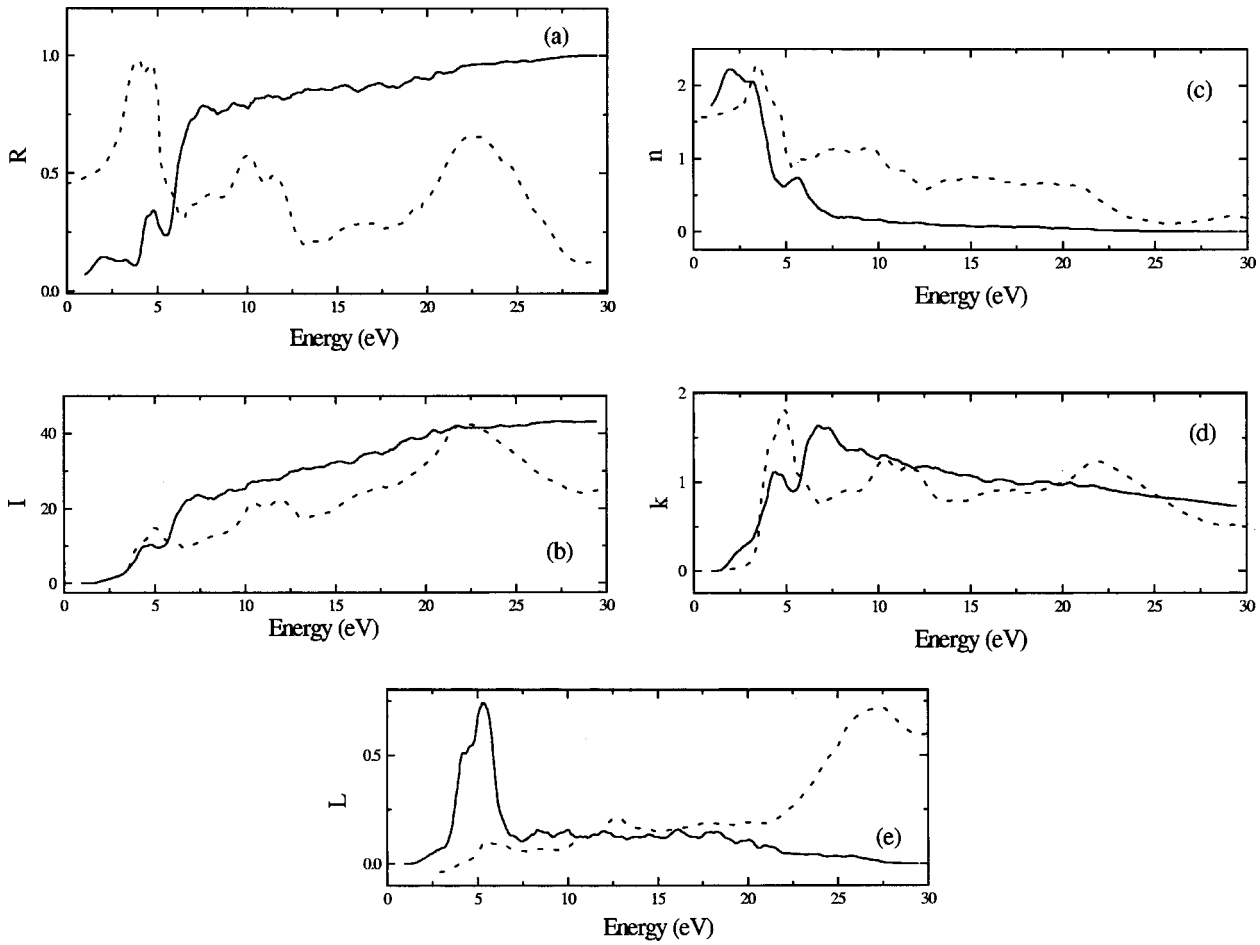

FIG. 8. The calculated optical parameters for paraelectric $BaTiO_3$ along with the experimental results (Ref. 8), (a) the reflectivity spectrum $R(\omega)$, (b) the absorption coefficient $I(\omega)$, (c) the refractive index $n(\omega)$, (d) the extinction coefficient $k(\omega)$, and (e) the energy-loss spectrum $L(\omega)$: dotted line is experimental, continuous line is theoretical.

is zero at the valence-band maximum but rises strongly with increasing binding energy. Conversely the O $2p$ contribution rises from zero at the conduction band minimum with increasing energy. These reflect the Ti $3d$-O $2p$ covalency.

B. Chemical bonding

In the previous section, it has been shown that there exists a significant hybridization of Ti $3d$ with O $2p$ states in $BaTiO_3$. This means that the bonding in this system cannot be purely ionic but must exhibit a large covalent part. To have a clear picture about the nature of chemical bonding between the constituent of $BaTiO_3$ in the paraelectric phase, we have shown the distribution of charge density in two different planes in Figs. 5 and 6. Figure 5 shows a sharing of charge between Ti and O due to Ti $3d$ and O $2p$ hybridization. Figure 6 shows the calculated valence charge density for cubic $BaTiO_3$. The distribution of charge around Ba site indicates that the bonding between Ba with TiO_3 is mainly ionic. Further the interatomic distance between the Ti and O is only 3.785 a.u. and that between Ba and O is 5.353 a.u. indicating the bonding between Ti and O is covalent in nature. To show the bonding between these units more clearly we have also plotted the corresponding three dimensional charge density map in the Figs. 5(b) and 6(b). From these figures it is clearly evident that substantial covalent bonding exists between Ti and O. It is to be mentioned here that if we consider the self-consistently calculated valence charges within different atomic spheres, the chemical formula for the system may roughly be written as $Ba^{-1.50}Ti^{+1.44}O_3^{+0.06}$. Thus we find a significant deviation from the charge distribution of a prototypical ionic crystal, namely, $A^{+2}B^{+4}O_3^{-6}$. Due to the strong hybridization between O p states and the Ti d states, there is a large amount of valence charge transfer back to Ti, revealing that the static Ti charge is significantly less than $+4$ and the O sphere is more or less neutral, rather than charged by -2. Similar results for $BaTiO_3$ have also been obtained by Cohen using the full-potential linearized augmented plane-wave method.[16,17]

C. Optical properties

The interband optical functions calculated using expressions (2) and (3) are shown in Figs. 7 and 8. The imaginary part $\epsilon''(\omega)$ of the complex dielectric constant $\epsilon(\omega)$ shows mainly two peaks at 3.8 and 5.9 eV. The first one is attributed to transitions from the O $2p$ (lower Γ_{15}) valence band to the Ti $3d$ ($\Gamma_{25'}$) conduction band (t_{2g}) and from the O $2p$ (upper Γ_{15}) valence band to the Ti $3d$ (Γ_{12}) conduction band (e_g). The second one is due to transitions from the O $2p$ (lower Γ_{15}) valence band to the Ti $3d$ (Γ_{12}) conduction band (e_g). These also explain the origin of the peak structure in

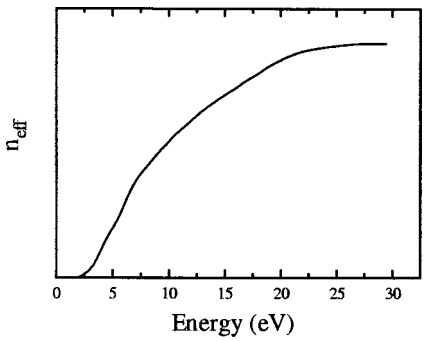

FIG. 9. The calculated effective number of electrons (n_{eff}) participating in the interband optical transitions.

the reflectivity $R(\omega)$ and the absorption coefficient $I(\omega)$ spectra. The energy-loss function $L(\omega)$ shows intense maxima at around 5 eV due to the excitation of plasmons. Absorption coefficient, energy loss, refractive index, and reflectivity spectra for $BaTiO_3$ crystals at room temperature (tetragonal phase) have been measured by several authors.[4,6,8] Since the effect of tetragonality on band structure has been found to be very small (10–150 meV),[4,27] we may compare our calculated values for optical functions with the room-temperature experimental results of Bauerle *et al.*[8] The experimental $\epsilon''(\omega)$ spectrum[8] deduced from reflectivity measurements by Kramers-Kronig analysis is mainly composed of two peak structures where the first peak is located at around 4 eV and the second one is located at around 10 eV. In Fig. 7 we have compared our calculated $\epsilon'(\omega)$ and $\epsilon''(\omega)$ spectra with the experimental[8] data. The calculated values agree well as regards the two-peak structure in the $\epsilon''(\omega)$ curve with a slight ($\sim$0.5 eV) shifting of the first peak from the experimental data while the second peak is shifted by about 4 eV from the experimental peak (Fig. 7). This discrepancy may be due to the inadequacy of the LDA as regards reproducing the band gap and the higher-energy excited states properly. Corrections like the ''scissors operator'' technique correct these discrepancies somewhat. Figures 8(a), 8(b), 8(c), 8(d), and 8(e) show a comparison of calculated and experimental[8] results for the reflectivity $R(\omega)$, absorption coefficient $I(\omega)$, refractive index $n(\omega)$, extinction coefficient $k(\omega)$, and energy loss $L(\omega)$, respectively. Overall, our theoretical spectra are found to be in good agreement with experimental data for lower energy range. The optical spectra generated using the theoretical lattice constant ($a = 7.43$ a.u.) remain almost the same.

In the energy-loss spectrum $L(\omega)$ in Fig. 8(e), it is seen that the calculated peak appears at about 5 eV whereas the experimental peak appears at about 27 eV. It is to be noted that the condition of plasma resonance is fulfilled at the energy where $\epsilon'(\omega)$ crosses zero. So the discrepancy as regards the peak of $L(\omega)$ arises because our calculated $\epsilon'(\omega)$ becomes zero at around 5 eV as shown in Fig. 7(a) whereas the experimental $\epsilon'(\omega)$ becomes zero at around 22 eV. The effective number of valence electrons per unit cell contributing in the interband transitions can be calculated by means of the sum rule

$$n_{\mathrm{eff}}(E_m) = \frac{2m}{Ne^2h^2}\int_0^{E_m} E\,\epsilon''(E)\,dE,$$

where E_m denotes the upper limit of integration. The quantities m and e are the electron mass and charge, respectively. N stands for the electron density. The results are shown in Fig. 9. The $n_{\mathrm{eff}}(E_m)$ reaches a saturation value above 25 eV. This shows that the deep-lying valence orbitals do not participate in the interband transition.

IV. CONCLUSIONS

We have made a detailed investigation of the electronic structure and optical properties of paraelectric $BaTiO_3$ in the cubic phase using the TB-LMTO method. The calculations show that the fundamental gap of $BaTiO_3$ is direct at the Γ point. Our calculated fundamental gap of 1.2 eV is smaller than the experimentally reported value 3.2 eV,[6] as it should be because of the discontinuity in the exchange correlation potential, which is not taken into account. Using the site and angular-momentum projected DOS and band structure we have analyzed the interband contribution to the optical properties. The chemical bonding of $BaTiO_3$ is also analyzed. The TiO_3 complex is bonded mainly by covalent bonds and the Ba and TiO_3 constituents are bonded ionically. The total DOS obtained from our first-principles calculation is compared with the experimental results.[9] We have examined the energy-dependent dielectric constants as well as related quantities such as reflectivities, absorption coefficients, energy-loss functions, refractive indices and extinction coefficients, and compared them with the experimental results[8] at room temperature for $BaTiO_3$ in the ferroelectric phase. Lastly, the effective number of electrons per unit cell participating in the interband transitions are calculated.

[1] M. E. Lines and A. M. Glass, *Principles and Applications of Ferroelectrics and Related Materials* (Clarendon, Oxford, 1977).

[2] R. T. Mara, G. B. B. Sutherland, and H. V. Tyrell, Phys. Rev. **96**, 801 (1954).

[3] W. G. Spitzer, R. C. Miller, D. A. Kleinman, and L. E. Howarth, Phys. Rev. **126**, 1710 (1962).

[4] M. Cardona, Phys. Rev. **140**, A651 (1965).

[5] A. Pinczuk, W. Taylor, and E. Burstein, Solid State Commun. **5**, 429 (1967).

[6] S. H. Wemple, Phys. Rev. B **2**, 2679 (1970).

[7] A. M. Quittet and M. Lambert, Solid State Commun. **12**, 1053 (1973).

[8] D. Bauerle, W. Braun, V. Saile, G. Sprussel, and E. E. Koch, Z. Phys. B **29**, 179 (1978).

[9] P. Pertosa, G. Hollinger, and F. M. Michel-Calendini, Phys. Rev. B **18**, 5177 (1978).

[10] F. Jona and G. Shirane, *Ferroelectric Crystals* (Macmillan, New York, 1962).

[11] R. Scharfschwerdt, A. Mazur, O. F. Schirmer, H. Hesse, and S.

Mendricks, Phys. Rev. B **54**, 15 284 (1996).
[12] B. D. Begg, E. R. Vance, and J. Nowotny, J. Am. Ceram. Soc. **77**, 3186 (1994).
[13] S. Schlag and H-F. Eicke, Solid State Commun. **91**, 883 (1994).
[14] B. D. Begg, K. S. Finnie, and E. R. Vance, J. Am. Ceram. Soc. **79**, 2666 (1996).
[15] O. K. Andersen and O. Jepsen, Phys. Rev. Lett. **53**, 2571 (1984).
[16] R. E. Cohen and H. Krakauer, Phys. Rev. B **42**, 6416 (1990).
[17] R. E. Cohen, Nature (London) **358**, 136 (1992).
[18] R. E. Cohen and H. Krakauer, Ferroelectrics **136**, 65 (1992).
[19] D. J. Singh and L. L. Boyer, Ferroelectrics **136**, 95 (1992).
[20] R. D. King-Smith and D. Vanderbilt, Phys. Rev. B **49**, 5828 (1994).
[21] R. D. King-Smith and D. Vanderbilt, Ferroelectrics **136**, 85 (1992).
[22] W. Kohn and L. J. Sham, Phys. Rev. **53**, 2571 (1965).
[23] U. von Barth and L. Hedin, J. Phys. C **5**, 1629 (1972).
[24] O. Jepsen and O. K. Andersen, Solid State Commun. **9**, 1763 (1971).
[25] P. Ravindran, A. Delin, B. Johansson, and O. Eriksson, Phys. Rev. B **59**, 1776 (1999).
[26] F. M. Michel-Calendini, H. Chermette, and J. Weber, J. Phys. C **13**, 1427 (1980).
[27] F. M. Michel-Calendini and G. Meslard, J. Phys. C **6**, 1709 (1973).